Article

# Single-Molecule Folding Mechanisms of the apo- and $Mg^{2+}$-Bound States of Human Neuronal Calcium Sensor-1

Mohsin M. Naqvi,[1,3] Pétur O. Heidarsson,[2] Mariela R. Otazo,[3,4] Alessandro Mossa,[5] Birthe B. Kragelund,[2,*] and Ciro Cecconi[1,3,*]

[1]Department of Physics, Informatics and Mathematics, University of Modena and Reggio Emilia, Modena, Italy; [2]Structural Biology and NMR Laboratory, Department of Biology, University of Copenhagen, Copenhagen N, Denmark; [3]CNR Institute of Nanoscience S3, Modena, Italy; [4]Department of Physics, Center of Applied Technologies and Nuclear Development (CEADEN), Miramar, La Habana, Cuba; and [5]Department of Physics, University of Bari and INFN, Sezione di Bari, Bari, Italy

ABSTRACT Neuronal calcium sensor-1 (NCS-1) is the primordial member of a family of proteins responsible primarily for sensing changes in neuronal $Ca^{2+}$ concentration. NCS-1 is a multispecific protein interacting with a number of binding partners in both calcium-dependent and independent manners, and acting in a variety of cellular processes in which it has been linked to a number of disorders such as schizophrenia and autism. Despite extensive studies on the $Ca^{2+}$-activated state of NCS proteins, little is known about the conformational dynamics of the $Mg^{2+}$-bound and apo states, both of which are populated, at least transiently, at resting $Ca^{2+}$ conditions. Here, we used optical tweezers to study the folding behavior of individual NCS-1 molecules in the presence of $Mg^{2+}$ and in the absence of divalent ions. Under tension, the $Mg^{2+}$-bound state of NCS-1 unfolds and refolds in a three-state process by populating one intermediate state consisting of a folded C-domain and an unfolded N-domain. The interconversion at equilibrium between the different molecular states populated by NCS-1 was monitored in real time through constant-force measurements and the energy landscapes underlying the observed transitions were reconstructed through hidden Markov model analysis. Unlike what has been observed with the $Ca^{2+}$-bound state, the presence of $Mg^{2+}$ allows both the N- and C-domain to fold through all-or-none transitions with similar refolding rates. In the absence of divalent ions, NCS-1 unfolds and refolds reversibly in a two-state reaction involving only the C-domain, whereas the N-domain has no detectable transitions. Overall, the results allowed us to trace the progression of NCS-1 folding along its energy landscapes and provided a solid platform for understanding the conformational dynamics of similar EF-hand proteins.

## INTRODUCTION

EF-hand calcium sensor proteins respond to cellular variations in calcium concentrations through conformational changes leading to activated states that interact with a large array of binding partners. Calcium binding in vivo occurs in the presence of a relatively constant 1000-fold excess of $Mg^{2+}$ ions and, perhaps unsurprisingly, many calcium-binding proteins also bind $Mg^{2+}$ under nonactivating concentrations of calcium (1,2). The role of $Mg^{2+}$ binding has been investigated for several EF-hand proteins. In the invertebrate sarcoplasmic calcium-binding proteins and troponin C, $Mg^{2+}$ binding to structural sites has been shown to be important for maintaining the structure of the proteins at any calcium concentrations (3). $Mg^{2+}$ binding has also been suggested to modulate $Ca^{2+}$ binding affinity of different proteins (4–6) and to switch off calcium-dependent signaling at resting $Ca^{2+}$ levels (2). Of importance, it is becoming increasingly clear that the $Mg^{2+}$-bound states of many EF-hand proteins have direct functional roles independent of calcium, underscored by the observation that the single EF-hand of the cytoplasmic C-terminal domain of the cardiac CaV1.2 channel only binds magnesium (7). The $Mg^{2+}$-bound state of the EF-hand protein DREAM (downstream regulatory element antagonist modulator) binds DNA targets in a sequence-specific manner, whereas binding of $Ca^{2+}$ disrupts this interaction (8). The $Mg^{2+}$-bound state of GCAP1 has been shown to activate retinal guanylyl cyclase (RetGC) in rod and cone cells (9). Moreover, and of relevance to the current study, the interactome of neuronal calcium sensor-1 (NCS-1) has been proposed to be modulated by ions, suggesting possible biological roles of the $Mg^{2+}$-bound state as well as of the apo state in neuronal functions (10).

NCS proteins are a family of EF-hand calcium-binding proteins expressed primarily in neurons, and NCS-1 is its primordial member. NCS-1 has its 190 amino acids comprised in four EF-hand motifs organized in two domains, where the N-domain (residues 1–95) consists of EF1 and EF2, and the C-domain (residues 96–190) of EF3 and EF4 (11). NMR spectroscopy and isothermal titration calorimetry have been used to confirm that EF2 and EF3 bind $Ca^{2+}$ and $Mg^{2+}$, whereas EF4 binds only $Ca^{2+}$ (4). EF1, on the other hand, is unable to bind ions due to a conserved Cys-to-Pro mutation (2). In humans, NCS-1 can

*Submitted November 7, 2014, and accepted for publication May 20, 2015.*

*Correspondence: ciro.cecconi@gmail.com or bbk@bio.ku.dk

Mohsin M. Naqvi and Pétur O. Heidarsson contributed equally to the work.

Editor: Nathan Baker.



0006-3495/15/07/0113/11 $2.00

http://dx.doi.org/10.1016/j.bpj.2015.05.028

interact with multiple and seemingly unrelated target proteins during the execution of its functions, both in a calcium-dependent and independent manner (12). The molecular basis of this multispecificity, exemplified by an interactome of >20 interaction partners reported to date, is currently unknown but suggests that NCS-1 can go through significant molecular rearrangements to accommodate different binding partners. NCS-1 has well-established functional roles such as regulating ion channels and G-protein-coupled receptors (13–15), membrane trafficking (16), and learning and neuronal growth (10). Several of these functions involve the $Mg^{2+}$-bound state, which interacts for example with the dopamine receptor D2 (13) and mediates the activation of P14K$\beta$ at resting cell conditions (17). Despite their obvious physiological importance, however, the structural features and conformational dynamics of the apo- and $Mg^{2+}$-bound states of NCS-1 are still poorly understood.

The $Ca^{2+}$-bound state of NCS-1 is well studied in terms of structure and has been shown, by x-ray crystallography and NMR spectroscopy, to have an open structure exposing large hydrophobic patches that mediate the interaction with most of its target proteins (18–20). Likewise, the folding mechanism of NCS-1 in the presence of $Ca^{2+}$ has been studied extensively using both traditional ensemble methods (4,19) and single-molecule experiments with optical tweezers (11,21). Through mechanical manipulation, we have recently characterized the energy landscape of the $Ca^{2+}$-bound state of NCS-1. These experiments revealed a sequential folding process where the C-domain first collapses into a partially folded structure and then undergoes a minor rearrangement to transit into its native conformation before the folding of the N-domain (11). We also showed that NCS-1 could become transiently kinetically trapped in two distinct misfolded states where pathologically high calcium concentrations increased the lifetimes of the misfolded structures (21). Although significant information is available on the structure, stability, and folding of NCS-1 in its $Ca^{2+}$-bound state, little is still known about its structural and dynamical properties in the absence of $Ca^{2+}$. Previous studies have suggested that the structure of the apo state of NCS-1 resembles that of a molten globule (22), and that upon $Mg^{2+}$ binding the protein adopts a closed form in which almost all hydrophobic regions are buried (4,23). Apart from this marginal information, however, the structural details of NCS-1 in the absence of divalent ions are still elusive and our mechanistic understanding of the conformational dynamics of the apo- and $Mg^{2+}$-bound states is highly limited.

Single-molecule techniques, such as optical tweezers, have proven powerful for dissecting the folding mechanisms of protein molecules, providing non-averaged information inaccessible to more traditional bulk techniques (24,25). Through mechanical manipulation it is nowadays possible to monitor in real time the dynamics of single proteins as they follow different routes and populate different intermediate states on their journey to the native structure (26–28). Analysis of the experimental data with advanced statistical methods allows the characterization of the kinetics and thermodynamics of the observed molecular transitions, and ultimately the reconstruction of the energy landscape of the protein (11,26,29,30). These studies have lately proved very useful for the description of the conformational dynamics of different proteins, revealing crucial information for a better understanding of the molecular mechanisms underlining their biological function (11,26,29–33).

Here, we use optical tweezers to characterize the folding processes of the apo- and $Mg^{2+}$-bound states of NCS-1 at the single molecule level. In the presence of $Mg^{2+}$, NCS-1 folds into an intermediate state consisting of a properly folded C-domain, and at lower forces it then transits to the native state through the folding of its N-domain. In contrast, in the absence of divalent ions, NCS-1 folds in a reversible two-state reaction involving only the C-domain with no observable transitions of the N-domain. Through constant-force measurements and hidden Markov model analysis the energy landscapes underlining the observed folding reactions were reconstructed. The results reported in this work shed light on the ion-dependent dynamics of NCS-1 and provide insights into the molecular basis of its conformational plasticity.

## MATERIALS AND METHODS

### Protein-DNA chimera preparation

To manipulate NCS-1 with optical tweezers we engineered double-cysteine constructs using either a wild-type pET-16b or a pseudowild-type pET-16b expression plasmid (with Cys-38 replaced by serine), by standard genetic techniques. The *Escherichia coli* strain BL21 (DE3) was used to express unmyristoylated each NCS-1 construct, and cells were grown at 37°C in Luria-Bertani medium. The protein was purified as described elsewhere (19,34), and attachment of DNA to proteins and coupling of protein-DNA chimeras to beads was performed exactly as in previous work (35).

### Force spectroscopy measurements

All measurements were carried out using a custom-built dual-beam optical tweezers setup that operates by direct measurement of light momentum (36,37). Measurements were performed either in 10 mM Tris, 250 mM NaCl, 10 mM $MgCl_2$, pH 7.0 or, to study the apo state of NCS-1, in the same buffer without $MgCl_2$ and with 0.5 mM EGTA. The DNA-protein chimeras were manipulated with a 3.10 $\mu$m antidigoxigenin-coated bead (Spherotec) held in the optical trap, and a 2.18 $\mu$m streptavidin-coated bead (Spherotec) held at the end of a micropipette by suction. The molecules were stretched and relaxed by moving the pipette toward the optical trap or away from it, respectively, by means of a piezoelectric flexure stage (MAX311/M, Thorlabs, Newton, NJ). Only those molecules displaying the characteristic DNA overstretching transition at 67 pN were used for acquiring data (29). In constant-speed experiments the data were acquired at a rate of 40 Hz, whereas in constant-force experiments at a rate of 100 Hz (36).

### Hidden Markov model (HMM) analysis

We used a HMM algorithm (38,39) to reconstruct from the constant-force hopping traces of our experiments the distribution (which we assume to be Gaussian) of the extension of each state and the transition probabilities between different states. The transition rate matrix K is computed from the transition probability matrix T by means of the relation $K = (\ln T)/\Delta t$, where $\Delta t = 0.01$ s for our data acquisition system. By collecting data obtained at different values of the force, we derive the chevron plots (see Figs. 2 *A*, 3 *F*, and 4 *F*, which we interpret according to the Kramers-Bell theory (40,41) to deduce the free energy differences among the states and the position of the barriers. The thermodynamics and kinetics information obtained in this way are summarized by the free-energy landscape sketch (see Fig. 2 *D*). Further details and references about HMM and the landscape reconstruction procedure are given in the Supporting Material.

## RESULTS

### Folding mechanism of the $Mg^{2+}$-bound state of NCS-1

Single NCS-1 molecules were manipulated as depicted in Fig. 1 *A*. DNA handles were attached to cysteine residues engineered at positions 4 and 188 and the protein was stretched and relaxed by moving the pipette relative to the optical trap. Typical force versus extension cycles for NCS-$1^{4\text{-}188}$ are depicted in Figs.1 *B* and S1.

During both stretching and relaxation, at a force of ~10 pN, the molecule populated an intermediate state *I*, located by extension halfway between the native (*N*) and the unfolded (*U*) states. At slow relaxation speed, fast fluctuations between *U* and *I* can be observed in a narrow range of forces. The C- and N-domains of NCS-1 consist of a similar number of residues and in the $Ca^{2+}$-bound state they unfold and refold sequentially (11). It is thus conceivable that the transitions observed in our experiments are the result of the sequential unfolding and refolding of the two domains. To confirm this, we analyzed 110 stretching traces with the wormlike chain (WLC) model of polymer elasticity (29,42,43) to estimate the change in contour length ($\Delta Lc$) associated with the different transitions. This analysis provided a $\Delta L_c$ of 30 ± 3 nm for the *N-I* transition, and a $\Delta L_c$ of 31 ± 2 nm for the *I-U* transition. These values are very close to the nominal $\Delta L_c$ for the unfolding of the C-domain ($\Delta L_c^0 = 33$ nm) and N-domain ($\Delta L_c^0 = 30$ nm) of the $Ca^{2+}$-bound state of NCS-1 (11) and are thus consistent with a sequential unfolding of the two domains in the $Mg^{2+}$-bound state. Nonetheless, the measured $\Delta L_c$ values are indistinguishable within the experimental errors and cannot be used for structural assignment. We thus investigated the behavior of two NCS-1 variants, NCS-$1^{10Gly}$ and NCS-$1^{38\text{-}188}$, where the size of the two domains was selectively altered. In NCS-$1^{10Gly}$ the size of the C-domain was increased by ~10% by inserting 10 glycine residues into an unstructured loop connecting EF3 and EF4. In NCS-$1^{38\text{-}188}$ one handle is attached to position 38 and force is applied to only 56 residues of the N-domain (from Ser-38

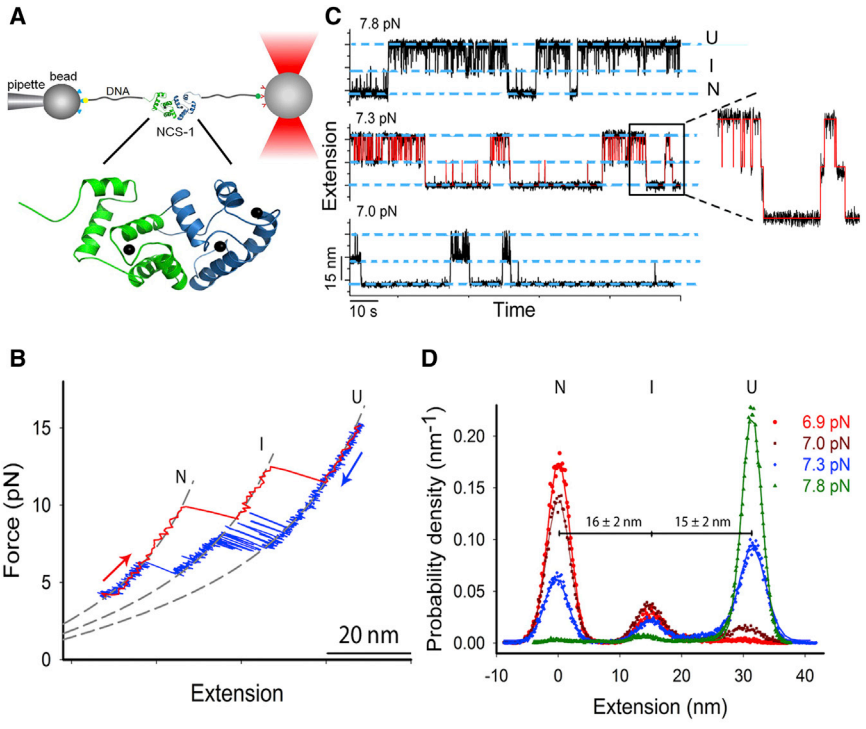


FIGURE 1 Folding transitions of the $Mg^{2+}$-bound state of NCS-1. (*A*) Sketch of the experimental setup. Single NCS-1 molecules were manipulated with functionalized polystyrene beads, as previously described (29,35), by means of DNA handles attached to unstructured terminal regions of the protein (position 4 and 188). The inset shows the solution structure of the $Ca^{2+}$-bound state of NCS-1 (PDB code 2LCP), with the N-domain represented in green and the C-domain in blue. $Ca^{2+}$ ions are shown as black dots. (*B*) Force versus extension cycle acquired by stretching (*red*, 100 nm/s) and relaxing (*blue*, 20 nm/s) a NCS-1 molecule in the presence of 10 mM $Mg^{2+}$. The native state (*N*) transits into the unfolded state (*U*) by populating an intermediate state (*I*), which is visited by the protein also during refolding. During the slow relaxation process fast fluctuations between *U* and *I* are detectable in a narrow range of forces. Color-coded arrows indicate the pulling (*red*) and relaxing (*blue*) directions. The stretching trace was fit to the WLC model (*dashed lines*) to estimate the changes in contour length associated to each unfolding transition. (*C*) Extension versus time traces for the $Mg^{2+}$-bound state of NCS-1, acquired at three different constant forces. The molecule hops between *N*, *I*, and *U* at equilibrium, with the unfolded state being increasingly populated at higher forces. A close-up view of the transitions in the dashed box is shown, along with the corresponding fit based on HMM (*red line*). (*D*) Probability density distributions (*symbols*) of the extensions of traces acquired at different constant forces. The distributions were fit to triple-Gaussian functions (*lines*) to estimate a change in extension of 16 ± 2 nm for the *N-I* transition and of 15 ± 2 nm for the *I-U* transition. To see this figure in color, go online.

to Arg-94), effectively reducing the size of the N-domain by ~40%. We analyzed 104 traces for NCS-1$^{38\text{-}188}$ (6 molecules), and 90 traces for NCS-1$^{10Gly}$ (4 molecules). Compared to NCS-1$^{4\text{-}188}$, both for unfolding and refolding, the high force transitions were longer in NCS-1$^{10Gly}$ (measured $\Delta L_c = 35 \pm 2$ nm; nominal $\Delta L_c{}^0 = 37$ nm) and the low force transitions shorter in NCS-1$^{38\text{-}188}$ (measured $\Delta L_c = 20 \pm 2$ nm; nominal $\Delta L_c{}^0 = 18$ nm) (Fig. S2). These data, along with the WLC model fitting results, suggest that the C-domain is mechanically more stable than the N-domain, and unfolds and refolds at higher forces. It is worth noticing that the results obtained with NCS-1$^{10Gly}$ are consistent only with the cooperative unfolding of EF3 and EF4 at high forces. In fact, with this mutant, an initial cooperative unfolding of EF2 and EF3, or of EF1 and EF4, would generate, in both cases, a larger unfolding transition at low forces (not at high forces), as the 10 glycines are placed in an unstructured loop between EF3 and EF4. The behavior of the $Mg^{2+}$-bound state of NCS-1 is consistent with that of its $Ca^{2+}$-bound state (11).

## Equilibrium unfolding/refolding transitions of the $Mg^{2+}$-bound state of NCS-1

The equilibrium unfolding/refolding processes of the $Mg^{2+}$-bound state of NCS-1 were characterized through constant force experiments, where the applied tension was kept constant by a feedback mechanism while the extension of the protein, as it jumped between different conformations, was monitored over time (Fig.1 *C*). We acquired 50 extension-time traces in the force range between 6.7 and 8.0 pN using 20 different molecules, and we analyzed each trace with a three-state HMM (44–46) to determine the force-dependent transition rates. The resulting data were fit to a linearized form of the Bell's model (40) to estimate the position of the transition states along the reaction coordinate and the zero force rates (Fig. 2 *A*). This analysis yielded a kinetic distance of 15 ± 1 nm between *N* and *I*, and a kinetic distance of 13 ± 1 nm between *I* and *U* (Table 1).

These distances compared well with the jumps in the molecule's extension observed in our constant-force traces (Fig. 1 *D*), showing the overall consistency of our HMM analysis. The dwell-time distributions of the *N*, *I*, and *U* states as determined from the HMM analysis could be well fitted to single exponentials, in agreement with the kinetics of two consecutive two-state processes (Fig. 2 *B*). To further characterize the thermodynamics of the observed transitions we analyzed the force-dependence of the occupation probability of each molecular state, Fig. 2 *C* (see Supporting Material for details). The results of this analysis (the equilibrium force $F_{1/2}$, the change in free energy $\Delta G$, and the distances between the states) are in agreement with those of the HMM analysis (Table 2). From the rates and transition state positions, the salient features of the energy landscape of the $Mg^{2+}$-bound state of NCS-1 at the equilibrium force $F_{1/2}$ were reconstructed (Fig. 2 *D*). The total change in free energy between *N* and *U* at zero external force ($\Delta G_{N\text{-}U}$), calculated by extrapolating from the force-dependent rates in Fig. 2 *A* and subtracting the free energy reduction of the unfolded state due to tethering (11,47), was −16 ± 3 kcal/mol (Supporting Material). This value compared well with the $\Delta G_{N\text{-}U}$ of −11 ± 2 kcal/mol measured in bulk experiments (Fig. S3) and with the $\Delta G_{N\text{-}U}$ of −16 ± 3 kcal/mol determined from the force-dependence of the occupation probabilities (Fig. 2 *C* and Supporting Material), showing the overall consistency of our analysis.

## Folding mechanism of the apo state of NCS-1

To investigate the effect of $Ca^{2+}$ and $Mg^{2+}$ on the folding process of NCS-1, we performed constant-velocity experiments in the absence of divalent ions. Remarkably, under these experimental conditions, the apo-protein unfolds and refolds reversibly in a two-state process near 6.5 pN, displaying fast fluctuations between two different molecular extensions, Fig. 3 *A*.

The change in contour length associated with the unfolding/refolding events was 31 ± 2 nm, suggesting that only half of the protein, possibly only one domain, gave rise to the observed transitions. The thermodynamics and kinetics of the bistability displayed by the molecule around 6.5 pN was analyzed through constant force experiments (Fig. 3 *B*). 52 extension-time traces from 12 different molecules were acquired in the force range between 5.7 and 7.2 pN. In each trace, the protein hopped between two distinct conformations differing in extension by 14 ± 1 nm (Fig. 3 *C*). The more extended (*unfolded*) one was favored by high forces. The lifetime distributions of both conformations could be well fitted by single exponentials (Fig. 3 *D*), and the unfolding probability displayed a sigmoidal dependence on force (Fig. 3 *E*); these data are consistent with a two-state unfolding/refolding mechanism. The transition rates and position of the transition state were estimated by fitting each time-extension trace with a two-state HMM (Fig. 3 *B*; Table 3).

From the position of the transition state we deduced a difference in extension between the folded and unfolded states of 14 ± 1 nm, which compared well with the experimental values (Fig. 3 *C*). Using the kinetic parameters of Table 3 we reconstructed the energy landscape of the molecule at $F_{1/2}$. After correction for the free energy loss of the unfolded state due to tethering (Supporting Material), we estimated a $\Delta G_{U\text{-}N}$ of 7 ± 1 kcal/mol, which compared well with the $\Delta G_{U\text{-}N}$ of 6 ± 1 kcal/mol measured in bulk experiments (Fig. S4), and with the $\Delta G_{U\text{-}N}$ of 8.5 ± 1.4 kcal/mol estimated from the unfolding probability (Fig. 3 *E*), thereby supporting the robustness of the HMM analysis.

The C-domain of NCS-1 has proved to be mechanically more resistant (11) and thermodynamically more stable (19) than the N-domain, and it is thus conceivable that the

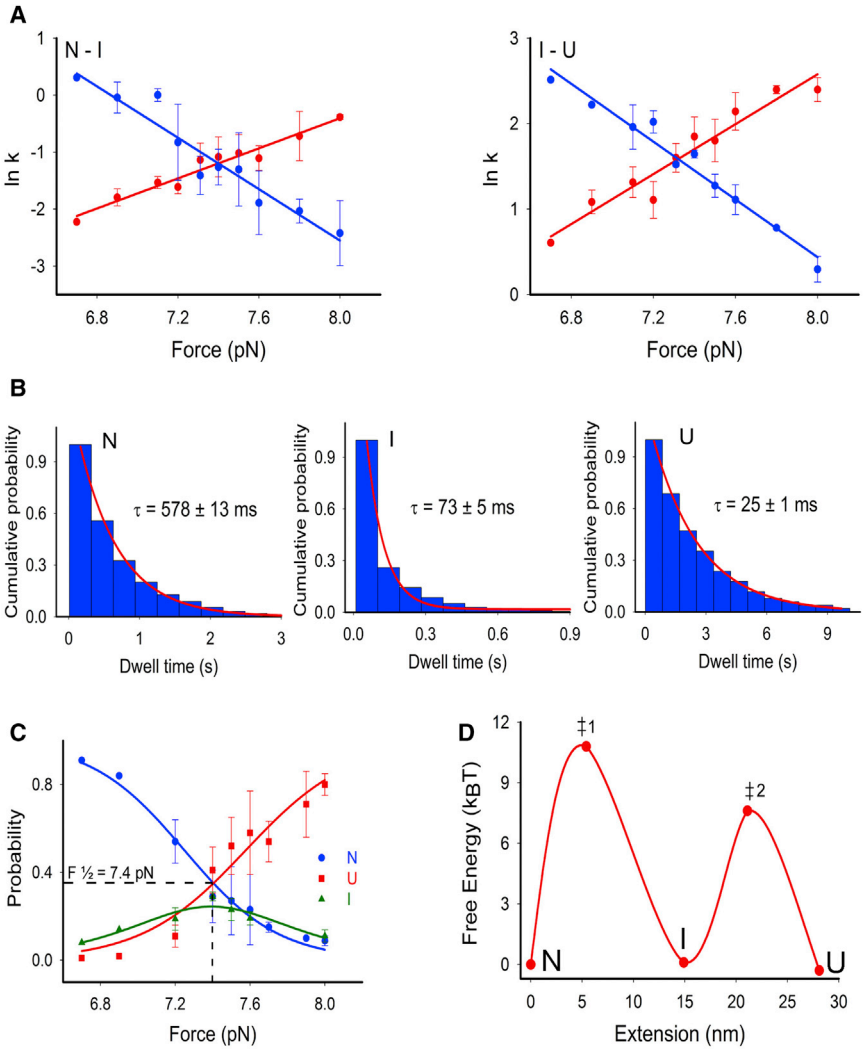


FIGURE 2 Energetics and kinetics of the $Mg^{2+}$-bound state of NCS-1. (*A*) Unfolding (*red*) and refolding (*blue*) rate constants for the *N-I* (*left*) and *I-U* (*right*) transitions estimated from extension-time traces acquired at different forces. Error bars represent standard deviations. The data were fit to the Bell's model (*solid lines*) to estimate the positions of the transition states and the zero force rates. (*B*) The dwell-time distributions of the *N*, *I*, and *U* states follow single exponential distributions. (*C*) Force-dependence of the occupation probability of the *N*, *I*, and *U* states (*color coded*), and their corresponding fits based on a two-state model (Supporting Material). The best fit values for the differences in extension and free energy between *N* and *U*, $\Delta X_{N\text{-}U} = 31.2 \pm 2.6$ nm and $\Delta G_{N\text{-}U} = 16.6 \pm 2.8$ kcal/mol, are in agreement with the results of the HMM analysis, Tables 1 and 2. The equilibrium force ($F_{1/2} = 7.4$ pN) corresponding to a probability of 0.33 is indicated. (*D*) Sketch of the free-energy landscape of the $Mg^{2+}$-bound state of NCS-1 at $F_{1/2}$. The positions and free energies of the *U*, *I*, *N*, and transition states (dagger1 and dagger2) are shown. To see this figure in color, go online.

reversible fluctuations observed in Fig. 3 *A* originate from the unfolding and refolding of the C-domain only. To test this hypothesis we pulled on the mutant NCS-$1^{95\text{-}188}$, where the cysteine at position 4 is moved to position 95 to effectively apply force only on the C-domain. The resulting force-extension traces showed reversible two-state unfolding/refolding transitions near 6.5 pN that closely resembled those observed when pulling on the entire molecule (Fig. 4 *A*), with very similar changes in contour length ($\Delta L_c = 32 \pm 2$ nm).

In fact, the unfolded and folded states of NCS-$1^{95\text{-}188}$ in the constant force measurements (Fig. 4 *B*) showed the same extensions (Fig. 4 *C*), energies (Fig. 4 *E*), and transition rates (Fig. 4 *F*) of the corresponding states of NCS-$1^{4\text{-}188}$, revealing nearly identical energy landscapes for the two variants in the absence of divalent ions (Fig. 4 *G*). In keeping with these conclusions, when force was applied only on the N-domain (NCS-$1^{4\text{-}95}$ mutant) under apo conditions, no discontinuities (*rips*) were observed in our force versus extension cycles, Fig. S5. These results clearly showed that the unfolding and refolding events displayed by NCS-1 in the absence of divalent ions originated only from the C-domain, suggesting that under these experimental conditions the N-domain is either unstructured, or only loosely folded,

**TABLE 1 Kinetic parameters of the folding reactions of the $Mg^{2+}$-bound state of NCS-1**

| Transition | $x_u$ (nm) | $x_f$ (nm) | $k^0{}_u$ ($s^{-1}$) | $k^0{}_f$ ($s^{-1}$) | $k_{1/2}$ ($s^{-1}$) | $\triangle G^{\ddagger}_{1/2}/k_BT$ |
|---|---|---|---|---|---|---|
| *N-I* | 5.4 ± 0.8 | 9.5 ± 0.8 | 2 (±0.8) × $10^{-5}$ | 5.4 (±0.8) × $10^{6}$ | 0.31 (±0.8) | 10.8 ± 1.1 |
| *I-U* | 6.2 ± 0.5 | 7 ± 0.5 | 1.1 (±1) × $10^{-4}$ | 1.1 (±1) × $10^{6}$ | 4.98 (±0.2) | 7.5 ± 0.98 |

The positions of the transition state for the unfolding and refolding reactions ($x_u$ *and* $x_f$, respectively), and the rates at zero force ($k^0{}_u$ *and* $k^0{}_f$, respectively) were estimated from the force-dependence of the transition rates. The transition rate and the activation free energy at $F_{1/2}$ are indicated as $k_{1/2}$ and $\Delta G^{\ddagger}_{1/2}$, respectively. Errors are estimated from fit parameters' uncertainties. $k_BT = 0.6$ kcal/mol.

**TABLE 2 Thermodynamic parameters of the folding reactions of the apo- and $Mg^{2+}$-bound states of NCS-1**

| NCS-1 variant | $\Delta G_{N\text{-}U}$ (kcal/mol) | $\Delta X_{N\text{-}U}$ (nm) |
|---|---|---|
| $Mg^{2+}$-bound NCS-$1^{4\text{-}188}$ | 16.6 ± 2.8 | 31.2 ± 2.6 |
| Apo NCS-$1^{4\text{-}188}$ | 8.5 ± 1.4 | 15 ± 1.5 |
| Apo NCS-$1^{95\text{-}188}$ | 5.96 ± 0.94 | 14.8 ± 2.3 |

The change in free energy and extension between the folded and unfolded states ($\Delta G_{N\text{-}U}$ and $\Delta X_{N\text{-}U}$, respectively) were estimated from the force-dependence of the occupation probabilities of the different molecular states. Errors are estimated from fit parameters' uncertainties.

and when stretched it unravels through transitions that are not detectable in our recordings. These data are quite similar to those obtained with the apo state of calmodulin, where only one domain exhibits reversible two-state transitions that can be easily observed in the force-extension curves, whereas the other gives rise to a signal that can only be vaguely inferred at very low forces (33).

The unfolding and refolding processes of the $Mg^{2+}$-bound and apo states of NCS-1 are schematically depicted in Fig. 5.

## DISCUSSION

Many members of the vast superfamily of EF-hand calcium-binding proteins populate $Mg^{2+}$-bound states. Some of these states have distinct structural roles, where the binding of $Mg^{2+}$ maintains the structure in the absence of $Ca^{2+}$ and presumably protects against aggregation or premature degradation, whereas others have a direct functional role. In the case of NCS-1, the $Mg^{2+}$-bound state is the primary interacting conformation for many of its targets (10,11) and its ion-dependent conformational dynamics therefore represents an important part of its functional repertoire. Our characterization of the folding of NCS-1 in the $Mg^{2+}$-bound and apo states reiterates our previous results obtained on the $Ca^{2+}$-bound state and show that the two EF-domains appear to fold as separate units regardless of ionic conditions. Using our results, we can now start to trace the progression of fold for NCS-1, from the likely transiently populated apo state, to resting $Ca^{2+}$ levels in a predominantly $Mg^{2+}$-bound state, to a fully $Ca^{2+}$-activated molecule during transient or sustained calcium elevation in neurons. The

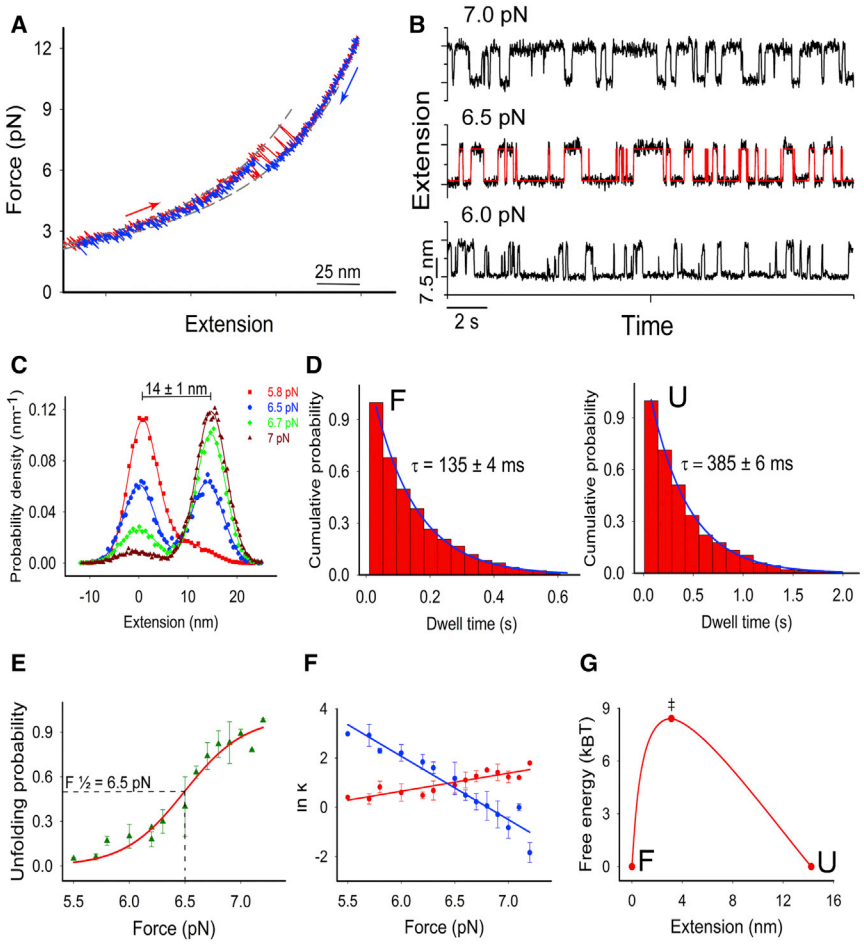


FIGURE 3 Folding transitions of the apo state of NCS-1. (*A*) Force-extension cycle acquired by stretching (*red*) and relaxing (*blue*) a NCS-1 molecule in the presence of no divalent ions. Around 6.5 pN the molecule displays bistability, fluctuating between two different molecular conformations. The associated changes in contour lengths ($\Delta L_c = 31 \pm 2$ nm) indicate that the discontinuities (*rips*) observed in the recorded traces are due to the unfolding and refolding of only half of the protein, the rest of the molecule giving rise to no detectable transitions. (*B*) Time-extension traces acquired at the indicated constant forces. The protein hops at equilibrium between a compact (*folded*) and an extended (*unfolded*) conformation, with the latter one being favored at higher forces. The data were analyzed with a two-state HMM, which produced idealized state transition traces like the one shown in red at 6.5 pN. (*C*) Extension probability density distributions of traces acquired at four different forces, and their corresponding double-Gaussian fittings (*solid lines*). The folded and unfolded states of the apo state of NCS-1 differ in extension by 14 ± 1 nm, and are equally populated at 6.5 pN. (*D*) Dwell-time distributions of the unfolded and folded states at 6.2 pN and their corresponding single exponential fittings. (*E*) Force-dependence of the occupation probability of the folded state and the corresponding two-state fitting. The best fit values, $\Delta X_{N\text{-}U} = 15 \pm 1.5$ nm and $\Delta G_{N\text{-}U} = 8.5 \pm 1.4$ kcal/mol, are in agreement with the results of the HMM analysis, Tables 2 and 3. The equilibrium force ($F_{1/2} = 6.5$ pN) corresponding to a probability of 0.5 is indicated. (*F*) Unfolding (*red*) and refolding (*blue*) rate constants at different forces as determined from the HMM analysis, and fits with the Bell model (*solid lines*). Error bars represent standard deviations. (*G*) Sketch of the free-energy landscape of NCS-1 at $F_{1/2}$ in the presence of no divalent ions, reconstructed using the HMM analysis. To see this figure in color, go online.

**TABLE 3 Kinetic parameters of the folding transitions of the apo state of NCS-1**

| NCS-1 variants | $x_u$ (nm) | $x_f$ (nm) | $k_u^0$ ($s^{-1}$) | $k_f^0$ ($s^{-1}$) | $k_{1/2}$ ($s^{-1}$) | $\Delta G^{\ddagger}_{1/2}/k_BT$ |
|---|---|---|---|---|---|---|
| $NCS1^{4-188}$ | 3.13 ± 0.4 | 11.1 ± 0.6 | 0.02 (±0.6) | 8.9 (±1) – $10^7$ | 2.72 (±0.3) | 8.4 ± 0.6 |
| $NCS1^{95-188}$ | 3.3 ± 0.4 | 10.7 ± 0.7 | 0.01 (±0.6) | 3.9 (±1) × $10^7$ | 2.0 (±0.3) | 8.7 ± 0.6 |

The kinetic quantities were measured from the force-dependence of the transition rates. Errors are estimated from fit parameters' uncertainties. $k_BT$ = 0.6 kcal/mol.

C-domain can already fold under apo conditions and is stabilized further by binding of $Mg^{2+}$, forming an intermediate state followed by $Mg^{2+}$-assisted folding of the N-domain into the $Mg^{2+}$-bound conformation. During transient or sustained elevation of $Ca^{2+}$, the molecule goes through a conformational change from a $Mg^{2+}$-bound state into a $Ca^{2+}$-activated state, where the largest structural changes are likely to be a consequence of the binding of $Ca^{2+}$ into the ion free EF4, which could involve a reorientation of the structural domains for tighter coupling to expose the hydrophobic crevice, as in the related NCS protein recoverin (48). Whether or not this involves unfolding and subsequent $Ca^{2+}$-assisted refolding or conformational changes within a competitive ion-exchange process is not known from our current data. Nonetheless, as shown in this work, the energy landscape of the protein significantly changes depending on the ionic environment to which it is exposed.

## The $Mg^{2+}$-bound state of NCS-1

Our results indicate that $Mg^{2+}$ promotes even more structuring than was previously proposed from NMR experiments (4). These latter studies suggested that $Mg^{2+}$ binding led to considerably less structuring than $Ca^{2+}$ binding as significant signal broadening was observed in the heteronuclear single-quantum coherence ($^1H$-$^{15}N$-HSQC) spectrum of NCS-1 and many peaks were missing, indicating conformational exchange (4). Remarkably, in this

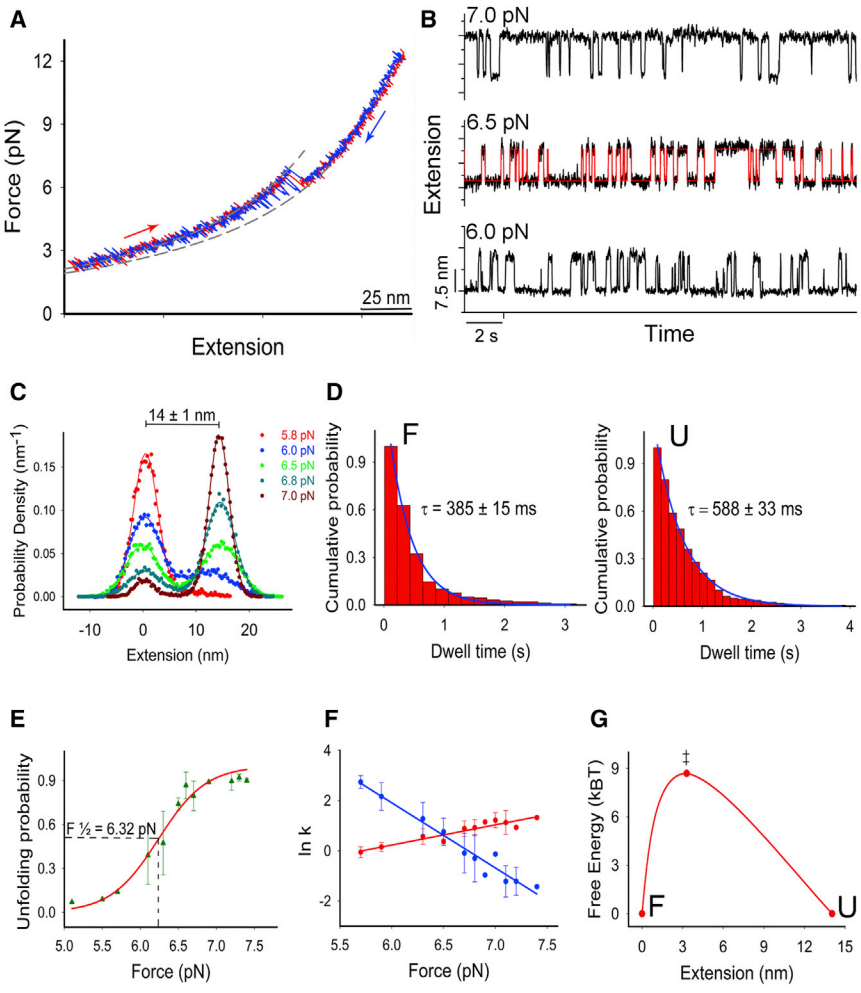


FIGURE 4 Folding transitions of $NCS\text{-}1^{95\text{-}188}$ in the absence of divalent ions. (*A*) Under these experimental conditions, when stretched (*red trace*) and relaxed (*blue trace*), $NCS\text{-}1^{95\text{-}188}$ displays reversible two-state fluctuations (*A*) that closely resemble those observed with $NCS\text{-}1^{4\text{-}188}$. In fact, when held at constant force (*B*), $NCS\text{-}1^{95\text{-}188}$ hops between two molecular conformations that are equal within experimental error to those described in Fig. 3, in terms of extensions (*C*), dwell-time distributions (*D*), force-dependent unfolding probability (*E*), and transition rates (*F*), Tables 2 and 3. Error bars represent standard deviations. It follows that, in the absence of divalent ions, the energy landscape of $NCS\text{-}1^{95\text{-}188}$ (*G*) is nearly identical to that of $NCS\text{-}1^{4\text{-}188}$. To see this figure in color, go online.

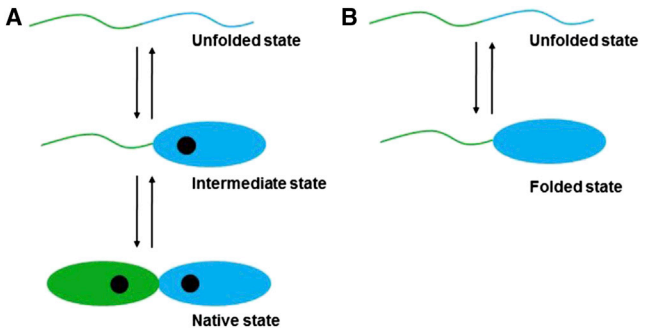


FIGURE 5 Schematic representation of the unfolding and refolding processes of the $Mg^{2+}$-bound (*A*) and apo (*B*) states of NCS-1. The N- and C-domains are shown as green and blue ellipses, respectively, and $Mg^{2+}$ ions are shown as black circles. To see this figure in color, go online.

respect, the near-UV CD spectrum of NCS-1, which reports primarily on tertiary structure, does not change much upon $Mg^{2+}$ binding to the apo state, whereas $Ca^{2+}$ binding causes drastic changes (4). It is therefore quite surprising that our results indicate that the entire N-domain obtains structure upon $Mg^{2+}$ binding; at least it is compacted to a state similar in shape as the $Ca^{2+}$-loaded state with unknown heterogeneity. However, even though the N-domain is unfolded under apo conditions in our accessible experimental force range (>2 pN), it cannot be excluded that it folds to a compact state at forces approaching zero. The mechanical properties of the $Mg^{2+}$-bound state closely resemble those of the $Ca^{2+}$-bound state. The N- and C-domains unfolds at forces ($9 \pm 1.2$ pN and $12 \pm 1.5$ pN, respectively) that are only slightly lower than those observed with NCS-1 in the presence of $Ca^{2+}$ ($10.6 \pm 0.6$ pN and $13.8 \pm 1$ pN, respectively), and the associated changes in contour length are equal within the experimental error in the two cases. These data suggest that $Mg^{2+}$ binding leads to a compact structure for NCS-1. It might also be that $Mg^{2+}$ binding leads to a closed conformation that resembles that sampled by the apo state of NCS-1, at least for the C-domain. $Mg^{2+}$ likely restricts the conformational space of the N-domain, but the dynamics of the ion-free EF4 could still lead to conformational exchange, reconciling at least some of the conflicting results obtained with NCS-1. In fact, almost 75% of the expected peaks are visible in the $^{1}H$-$^{15}N$-HSQC of myristoylated NCS-1 (120 out of 174 (4)), consistent with one out of four EF-hands experiencing conformational exchange. We envision that $Mg^{2+}$ binding leads to a fully compact globular yet dynamic structural ensemble with a partially open binding site and $Ca^{2+}$ binding leads to reorientation and docking of the two domains adding an additional stability term, and exposing fully the binding site. This is discussed further below.

The folding reactions of the $Mg^{2+}$- and $Ca^{2+}$-bound states of NCS-1 share common features, but also display remarkable differences. In both cases, the N-domain folds via a two-state process, crossing transition-state barriers located at comparable positions along the reaction coordinate (11). Conversely, the C-domain follows quite different folding pathways depending on the ionic environment. In the presence of $Mg^{2+}$, the C-domain folds through a single all-or-none reaction, with a rate constant ($k^0_f$) of ~$10^6$ $s^{-1}$. In contrast, in the presence of $Ca^{2+}$, the C-domain folds first into a partially folded conformation and then transits into its native state through a rate-limiting transition ($k^0_f$ ~38 $s^{-1}$) that involves calcium binding into the EF4 site. This latter process slows down the overall folding rate by several orders of magnitude and is linked to NCS-1's misfolding (21). These data suggest that in neurons, NCS-1 folds into its native structure more efficiently and safely at resting $Ca^{2+}$ levels in a predominantly $Mg^{2+}$-bound state, compared to its folding occurring during $Ca^{2+}$elevation.

## The apo state of NCS-1

Our results suggest that in the absence of divalent ions NCS-1 has a folded C-domain and an unstructured N-domain. One obvious difference between the two domains is a conserved Cys-Pro mutation in the N-domain that renders EF1 unable to bind divalent ions (19). It is well known that EF-hands are commonly found in pairs and binding of ions makes the EF-domain pair stable. For NCS-1, however, the folding or unfolding of the EF-hand pairs seems conserved even in the absence of ions, as the EF-hands of the N- and C-domains are either both folded or unfolded, displaying a considerable cross talk between them.

In the apo state, NCS-1 has been previously shown to have significant secondary structure yet little tertiary structure, and the $^{1}H$-$^{15}N$ HSQC spectrum has been shown to be severely signal broadened, suggesting a lack of stable structures (4,22). Our equilibrium unfolding data (Fig. S3) show an early decrease in fluorescence intensity at very low denaturant concentration. This decrease occurs gradually, lacking a pretransition baseline, and indicates the unfolding of a structure with only marginal tertiary interactions, followed by a cooperative unfolding transition. These data acquired in bulk appear to be consistent with our single molecule data. In fact, under tension and in the absence of divalent ions, NCS-1 unfolds and refolds through reversible two-state transitions that involved only the C-domain. The collapsed state of the N-domain suggested by the equilibrium unfolding experiments may be too unstable to be observable in the force range used in our experiments. We notice that the behavior under tension of the apo state is clearly different from that displayed by the $Mg^{2+}$- and $Ca^{2+}$-bound states of NCS-1 and by other native state structures stabilized by tertiary contacts, which unfold and refold out of equilibrium through transitions accompanied by hysteresis (11,30,36,49). On the basis of our data, we speculate that the apo state of NCS-1 consist of a highly dynamic ensemble of similar structures, stabilized by weak interactions, which interconvert on intermediate NMR timescales,

giving rise to the observed signal broadening in the HSQC spectrum (4), and to the reversible transitions in single molecule experiments. Thus, similar to intrinsically disordered proteins (50) and to that of the calcium binding S100 proteins (51), neural calcium sensors may exploit ligand-driven folding upon binding to drive the thermodynamics for binding and the selection of binding partners.

### Functional, ion-dependent dynamics of NCS-1

NCS-1 has a broad interactome currently consisting of >20 reported binding partners (52). The different protein partners can be bound predominantly in either domain or both at the same time, in either a calcium-dependent or independent manner. This multispecificity requires a certain degree of conformational plasticity that is poorly understood on the molecular level. The different stabilities and folding rates of the two domains may reflect the conformational heterogeneity needed to allow for accommodation of multiple different ligands in the binding pocket, which spans through both domains. In addition, NCS-1 can gain functional versatility not only through the full or partial folding or unfolding of the two EF-domains but also through their coupling or decoupling, which affects their relative orientation and dynamics. This allostery may fine-tune the exposure of the binding sites for the various interaction partners of NCS-1.

The interaction of NCS-1 with the D2 dopamine receptor (D2R) is believed to include both the $Mg^{2+}$-bound and $Ca^{2+}$-bound states (13). NCS-1 interacts with the C-terminal tail residues of D2R independent of calcium and upon calcium activation it binds the G-protein-coupled receptor kinase (GRK2) and partially inhibits it from phosphorylating the third intracellular loop of D2R, thus being responsible for its desensitization (13). Presumably, D2R and GRK2 are bound to separate NCS-1 domains. No detailed structural information on the interactions is available but biochemical and structural models have suggested different scenarios regarding the stoichiometry and domain involvement in binding (53,54). Our results indicate that the extension and folding rate of the N-domain is similar in its $Mg^{2+}$-bound and $Ca^{2+}$-bound states. It could therefore be speculated that the N-domain is responsible for binding D2R because its properties may not change much when transiting from $Mg^{2+}$ to $Ca^{2+}$ conditions. Upon calcium activation, the N-domain-D2R interaction may become tighter and the conformational changes of the C-domain, mostly through binding of calcium into EF4, enable further coupling with the N-domain, which may fully expose the second binding site for GRK2. This would be consistent with evidence which suggest that occupancy of calcium in EF2 is sufficient for the NCS-1-D2R interaction (54). In this respect, an important next step to understand these processes in detail will be to directly observe and characterize the activation of NCS-1 from a predominantly $Mg^{2+}$-bound state to the fully calcium-bound state. This would elucidate for example whether it is possible to traverse directly from an $Mg^{2+}$-bound state to a $Ca^{2+}$-bound state, or whether partial or full unfolding is a prerequisite for calcium activation. This will be especially important for the D2R-NCS-1 interaction because NCS-1 has been suggested as a potential target for antipsychotic drugs (55). To this end our results on the conformational dynamics of NCS-1 may form a platform for drug design.

## CONCLUSIONS

In conclusion, we have determined the salient features of the folding free-energy landscapes of the $Mg^{2+}$-bound and apo states of NCS-1. We found these states to have distinct folding properties from the calcium-bound state, where NCS-1 in the presence of magnesium folds each domain separately through all-or-none transitions, whereas in the apo state it only folds its C-domain while the N-domain remains unfolded or highly destabilized. We found that the $Mg^{2+}$-bound state is more structured than previously described, displaying mechanical properties, cooperativity, and end-to-end distances that closely resemble those of the $Ca^{2+}$-bound state. Our results represent an important detailed decomposition of states for the deciphering of the complete conformational as well as functional dynamics of NCS-1.

## SUPPORTING MATERIAL

Supporting Materials and Methods and five figures are available at http://www.biophysj.org/biophysj/supplemental/S0006-3495(15)00540-8.

## AUTHOR CONTRIBUTIONS

M.M.N, P.O.H., B.B.K., and C.C. designed research; M.M.N, P.O.H., and M.R.O. performed experiments; A.M. contributed new analytic tools; B.B. contributed protein samples; M.M.N, P.O.H., A.M., M.R.O., and C.C. analyzed data; M.M.N. performed hidden Markov model analysis and M.M.N, P.O.H., A.M., B.B.K., and C.C. wrote the article.

## ACKNOWLEDGMENTS

P.O.H. and B.B.K. acknowledge the Carlsberg Foundation and the Lundbeck Foundation for financial support. C.C. gratefully acknowledges financial support from Fondazione Cassa di Risparmio di Modena, the EU through a Marie Curie International Re-Integration Grant (No. 44952), the Italian MIUR (grant No. 17DPXLNBEK), and partial support from Italian MIUR FIRB RBPR05JH2P "ITALNANONET". M.R.O. gratefully acknowledges financial support from the Abdus Salam International Centre for Theoretical Physics, of UNESCO and IAEA, (ICTP), TRIL program. Dr. Luca Bellucci and Dr. Stefano Corni are thanked for critical comments on the article.

## SUPPORTING CITATIONS

References (56–59) appear in the Supporting Material.

## REFERENCES


1. Gifford, J. L., M. P. Walsh, and H. J. Vogel. 2007. Structures and metal-ion-binding properties of the Ca2+-binding helix-loop-helix EF-hand motifs. *Biochem. J.* 405:199–221.
2. Grabarek, Z. 2011. Insights into modulation of calcium signaling by magnesium in calmodulin, troponin C and related EF-hand proteins. *Biochim. Biophys. Acta.* 1813:913–921.
3. Zot, H. G., and J. D. Potter. 1982. A structural role for the Ca2+-Mg2+ sites on troponin C in the regulation of muscle contraction. Preparation and properties of troponin C depleted myofibrils. *J. Biol. Chem.* 257:7678–7683.
4. Aravind, P., K. Chandra, …, Y. Sharma. 2008. Regulatory and structural EF-hand motifs of neuronal calcium sensor-1: Mg 2+ modulates Ca 2+ binding, Ca 2+ -induced conformational changes, and equilibrium unfolding transitions. *J. Mol. Biol.* 376:1100–1115.
5. Peshenko, I. V., and A. M. Dizhoor. 2006. Ca2+ and Mg2+ binding properties of GCAP-1. Evidence that Mg2+-bound form is the physiological activator of photoreceptor guanylyl cyclase. *J. Biol. Chem.* 281:23830–23841.
6. Wingard, J. N., J. Chan, …, J. B. Ames. 2005. Structural analysis of Mg2+ and Ca2+ binding to CaBP1, a neuron-specific regulator of calcium channels. *J. Biol. Chem.* 280:37461–37470.
7. Brunet, S., T. Scheuer, …, W. A. Catterall. 2005. Modulation of CaV1.2 channels by Mg2+ acting at an EF-hand motif in the COOH-terminal domain. *J. Gen. Physiol.* 126:311–323.
8. Osawa, M., A. Dace, …, J. B. Ames. 2005. Mg2+ and Ca2+ differentially regulate DNA binding and dimerization of DREAM. *J. Biol. Chem.* 280:18008–18014.
9. Peshenko, I. V., E. V. Olshevskaya, …, A. M. Dizhoor. 2010. Activation of retinal guanylyl cyclase RetGC1 by GCAP1: stoichiometry of binding and effect of new LCA-related mutations. *Biochemistry.* 49:709–717.
10. Burgoyne, R. D., and L. P. Haynes. 2012. Understanding the physiological roles of the neuronal calcium sensor proteins. *Mol. Brain.* 5:2.
11. Heidarsson, P. O., M. R. Otazo, …, C. Cecconi. 2013. Single-molecule folding mechanism of an EF-hand neuronal calcium sensor. *Structure.* 21:1812–1821.
12. Burgoyne, R. D. 2007. Neuronal calcium sensor proteins: generating diversity in neuronal Ca2+ signalling. *Nat. Rev. Neurosci.* 8:182–193.
13. Kabbani, N., L. Negyessy, …, R. Levenson. 2002. Interaction with neuronal calcium sensor NCS-1 mediates desensitization of the D2 dopamine receptor. *J. Neurosci.* 22:8476–8486.
14. Navarro, G., J. Hradsky, …, M. Mikhaylova. 2012. NCS-1 associates with adenosine A(2A) receptors and modulates receptor function. *Front. Mol. Neurosci.* 5:53.
15. Weiss, J. L., H. Hui, and R. D. Burgoyne. 2010. Neuronal calcium sensor-1 regulation of calcium channels, secretion, and neuronal outgrowth. *Cell. Mol. Neurobiol.* 30:1283–1292.
16. Haynes, L. P., G. M. Thomas, and R. D. Burgoyne. 2005. Interaction of neuronal calcium sensor-1 and ADP-ribosylation factor 1 allows bidirectional control of phosphatidylinositol 4-kinase beta and trans-Golgi network-plasma membrane traffic. *J. Biol. Chem.* 280:6047–6054.
17. Burgoyne, R. D., D. W. O'Callaghan, …, A. V. Tepikin. 2004. Neuronal Ca2+-sensor proteins: multitalented regulators of neuronal function. *Trends Neurosci.* 27:203–209.
18. Bourne, Y., J. Dannenberg, …, O. Pongs. 2001. Immunocytochemical localization and crystal structure of human frequenin (neuronal calcium sensor 1). *J. Biol. Chem.* 276:11949–11955.
19. Heidarsson, P. O., I. J. Bjerrum-Bohr, …, B. B. Kragelund. 2012. The C-terminal tail of human neuronal calcium sensor 1 regulates the conformational stability of the $Ca^{2+}$-activated state. *J. Mol. Biol.* 417:51–64.
20. Bellucci, L., S. Corni, …, E. Paci. 2013. The structure of neuronal calcium sensor-1 in solution revealed by molecular dynamics simulations. *PLoS ONE.* 8:e74383.
21. Heidarsson, P. O., M. M. Naqvi, …, C. Cecconi. 2014. Direct single-molecule observation of calcium-dependent misfolding in human neuronal calcium sensor-1. *Proc. Natl. Acad. Sci. USA.* 111:13069–13074.
22. Cox, J. A., I. Durussel, …, E. D. Gundelfinger. 1994. Cation binding and conformational changes in VILIP and NCS-1, two neuron-specific calcium-binding proteins. *J. Biol. Chem.* 269:32807–32813.
23. Kuboniwa, H., N. Tjandra, …, A. Bax. 1995. Solution structure of calcium-free calmodulin. *Nat. Struct. Biol.* 2:768–776.
24. Bustamante, C., Y. R. Chemla, …, D. Izhaky. 2004. Mechanical processes in biochemistry. *Annu. Rev. Biochem.* 73:705–748.
25. Ferreon, A. C., and A. A. Deniz. 2011. Protein folding at single-molecule resolution. *Biochim. Biophys. Acta.* 1814:1021–1029.
26. Heidarsson, P. O., M. M. Naqvi, …, C. Cecconi. 2013. Conformational dynamics of single protein molecules studied by direct mechanical manipulation. *Adv. Protein Chem. Struct. Biol.* 92:93–133.
27. Moffitt, J. R., Y. R. Chemla, …, C. Bustamante. 2008. Recent advances in optical tweezers. *Annu. Rev. Biochem.* 77:205–228.
28. Zoldák, G., and M. Rief. 2013. Force as a single molecule probe of multidimensional protein energy landscapes. *Curr. Opin. Struct. Biol.* 23:48–57.
29. Cecconi, C., E. A. Shank, …, S. Marqusee. 2005. Direct observation of the three-state folding of a single protein molecule. *Science.* 309:2057–2060.
30. Stigler, J., F. Ziegler, …, M. Rief. 2011. The complex folding network of single calmodulin molecules. *Science.* 334:512–516.
31. Schlierf, M., F. Berkemeier, and M. Rief. 2007. Direct observation of active protein folding using lock-in force spectroscopy. *Biophys. J.* 93:3989–3998.
32. Schlierf, M., H. Li, and J. M. Fernandez. 2004. The unfolding kinetics of ubiquitin captured with single-molecule force-clamp techniques. *Proc. Natl. Acad. Sci. USA.* 101:7299–7304.
33. Stigler, J., and M. Rief. 2012. Calcium-dependent folding of single calmodulin molecules. *Proc. Natl. Acad. Sci. USA.* 109:17814–17819.
34. Kragelund, B. B., A. Hauenschild, …, B. E. Finn. 2000. 1H, 13C, and 15N assignments of un-myristoylated Ca2+-frequenin, a synaptic efficacy modulator. *J. Biomol. NMR.* 16:85–86.
35. Cecconi, C., E. A. Shank, …, C. Bustamante. 2008. Protein-DNA chimeras for single molecule mechanical folding studies with the optical tweezers. *Eur. Biophys. J.* 37:729–738.
36. Heidarsson, P. O., I. Valpapuram, …, C. Cecconi. 2012. A highly compliant protein native state with a spontaneous-like mechanical unfolding pathway. *J. Am. Chem. Soc.* 134:17068–17075.
37. Smith, S. B., Y. Cui, and C. Bustamante. 2003. Optical-trap force transducer that operates by direct measurement of light momentum. *Methods Enzymol.* 361:134–162.
38. Petrie, L. E. B. T. 1966. Statistical inference for probabilistic functions of finite state Markov chains. *Ann. Math. Stat.* 37:1554–1563.
39. Rabiner, L. 1989. A tutorial on hidden Markov models and selected applications in speech recognition. *Proceedings of the IEEE.* 77:257–286.
40. Bell, G. I. 1978. Models for the specific adhesion of cells to cells. *Science.* 200:618–627.
41. Tinoco, Jr., I. 2004. Force as a useful variable in reactions: unfolding RNA. *Annu. Rev. Biophys. Biomol. Struct.* 33:363–385.
42. Bustamante, C., Z. Bryant, and S. B. Smith. 2003. Ten years of tension: single-molecule DNA mechanics. *Nature.* 421:423–427.
43. Bustamante, C., J. F. Marko, …, S. Smith. 1994. Entropic elasticity of lambda-phage DNA. *Science.* 265:1599–1600.
44. Chodera, J. D., P. Elms, …, N. S. Hinrichs. 2011. Bayesian hidden Markov model analysis of single-molecule force spectroscopy: Characterizing kinetics under measurement uncertainty. arXiv preprint arXiv:1108.1430.
45. Gao, Y., G. Sirinakis, and Y. Zhang. 2011. Highly anisotropic stability and folding kinetics of a single coiled coil protein under mechanical tension. *J. Am. Chem. Soc.* 133:12749–12757.

46. McKinney, S. A., C. Joo, and T. Ha. 2006. Analysis of single-molecule FRET trajectories using hidden Markov modeling. *Biophys. J.* 91:1941–1951.

47. Liphardt, J., B. Onoa, …, C. Bustamante. 2001. Reversible unfolding of single RNA molecules by mechanical force. *Science.* 292:733–737.

48. Yap, K. L., J. B. Ames, …, M. Ikura. 1999. Diversity of conformational states and changes within the EF-hand protein superfamily. *Proteins.* 37:499–507.

49. Shank, E. A., C. Cecconi, …, C. Bustamante. 2010. The folding cooperativity of a protein is controlled by its chain topology. *Nature.* 465:637–640.

50. Sugase, K., H. J. Dyson, and P. E. Wright. 2007. Mechanism of coupled folding and binding of an intrinsically disordered protein. *Nature.* 447:1021–1025.

51. Botelho, H. M., M. Koch, …, C. M. Gomes. 2009. Metal ions modulate the folding and stability of the tumor suppressor protein S100A2. *FEBS J.* 276:1776–1786.

52. Lian, L. Y., S. R. Pandalaneni, …, L. P. Haynes. 2014. Demonstration of binding of neuronal calcium sensor-1 binding to the cav2.1 p/q-type calcium channel. *Biochemistry.* 53:6052–6062.

53. Lian, L. Y., S. R. Pandalaneni, …, R. D. Burgoyne. 2011. Characterisation of the interaction of the C-terminus of the dopamine D2 receptor with neuronal calcium sensor-1. *PLoS ONE.* 6:e27779.

54. Woll, M. P., D. A. De Cotiis, …, J. M. Flanagan. 2011. Interaction between the D2 dopamine receptor and neuronal calcium sensor-1 analyzed by fluorescence anisotropy. *Biochemistry.* 50:8780–8791.

55. Kabbani, N., M. P. Woll, …, R. Levenson. 2012. Dopamine receptor interacting proteins: targeting neuronal calcium sensor-1/D2 dopamine receptor interaction for antipsychotic drug development. *Curr. Drug Targets.* 13:72–79.

56. Gebhardt, J. C., T. Bornschlögl, and M. Rief. 2010. Full distance-resolved folding energy landscape of one single protein molecule. *Proc. Natl. Acad. Sci. USA.* 107:2013–2018.

57. Maxwell, S. L., H. Y. Ho, …, M. Li. 2005. Pitx3 regulates tyrosine hydroxylase expression in the substantia nigra and identifies a subgroup of mesencephalic dopaminergic progenitor neurons during mouse development. *Dev. Biol.* 282:467–479.

58. Mossa, A., M. Manosas, …, F. Ritort. 2009. Dynamic force spectroscopy of DNA hairpins: I. Force kinetics and free energy landscapes. *J. Stat. Mech.* 2009:P02060.

59. Tinoco, Jr., I., and C. Bustamante. 2002. The effect of force on thermodynamics and kinetics of single molecule reactions. *Biophys. Chem.* 101-102:513–533.

## Supporting Material

# Single-molecule folding mechanisms of the apo- and $Mg^{2+}$-bound states of human Neuronal Calcium Sensor-1

**Mohsin M. Naqvi, Pétur O. Heidarsson, Mariela R. Otazo, Alessandro Mossa, Birthe B. Kragelund, and Ciro Cecconi**

**Hidden Markov Model analysis and landscape reconstruction**

Hidden Markov Model (HMM) techniques are a powerful statistical tool to analyze time series. The problem, frequently encountered in data analysis, is the following: assume that the system under investigation can be reasonably well approximated by a Markov chain with $n$ states and time-independent transition matrix $T_{ij}$ ($i, j = 1,\ldots,n$). Experiments made on the system can not directly assess which state the system is in (it is *hidden*), but each state emits a characteristic signal (either discretely or continuously distributed) which can be detected. From a sufficiently long time series of observations one can infer both the transition matrix elements and the characteristics of the signal emitted by each state, and then assign to each data point the most likely state of the system at that time. The algorithms to perform these reconstructions were first developed by mathematicians in the '60s (1) and then widely applied to artificial intelligence problems, notably speech recognition (2). Lately they have been adopted by the biophysical community as the tool of choice for analyzing data from single-molecule experiments, at first fluorescence (3) and then optical tweezers (4)

In our case, the states are N, I, U and the signal is the normally distributed end-to-end extension of the molecular construct protein + handles. From our HMM reconstruction, we estimate the elements of the transition matrix $T_{ij}$, which can be translated into transition rates using the formula $K_{ij} = (\ln M)_{ij}/\Delta t$, where $\Delta t$ is the time interval between two consecutive measurements (in our experiment, 0.01 s). By collecting rates at different force values we obtain the chevron plots in Figs. 2A, 3F, 4F. Such plots are interpreted according to the Kramers-Bell theory (5) in the simplified version of (6) (see also (7) for a proof of the validity of this approximation):

$$k_{\rightarrow}(f) = k_0 \exp\left[\frac{f x_{\rightarrow}^{\ddagger}}{k_B T}\right]$$

$$k_{\leftarrow}(f) = k_0 \exp\left[\frac{\Delta G - f x_{\leftarrow}^{\ddagger}}{k_B T}\right]$$

$$k_0(f) = k_m \exp\left[\frac{\Delta G^{\ddagger}}{k_B T}\right]$$

From the slopes of the linear fits (in semi-log scale) performed in the chevron plots we can therefore deduce the position of the barriers, while the intercepts give access to the free energy difference between the states. In order to present a free energy landscape like the one in Fig. 2D we need one more data: the pre-exponential factor $k_m$, which we cannot directly measure with our experimental apparatus. We adopt the value 1.2 $\times 10^{-4}$ Hz, which has been experimentally measured in a setting very similar to ours, albeit with a different protein (8).

**Thermodynamic Analysis of a three state system**

If we have a three state system with phases *N*, *I* and *U* then the partition function (equation 45 in reference (9) can be written as:

$$Z = exp\left(-\frac{\Delta G_U(T,x_U) - F x_U}{k_B T}\right) + exp\left(-\frac{\Delta G_I(T,x_I) - F x_I}{k_B T}\right) + exp\left(-\frac{\Delta G_N(T,x_N) - F x_N}{k_B T}\right) \quad (1)$$

Where $x_U$, $x_I$, $x_N$ are the average extensions of the three states at temperature *T*, atmospheric pressure and applied force *F*, while

$$\Delta G_U = G_U - G_0 \quad (2)$$

$$\Delta G_I = G_I - G_0 \quad (3)$$

$$\Delta G_N = G_N - G_0 \quad (4)$$

are the thermodynamic free energies at constant temperature, pressure and average extensions of the three states measured with respect to an arbitrary reference state. From the above relations the probability of a single molecule of being in state *N*, *I* and *U* at temperature *T* and force *F* are:

$$P_U = \frac{1}{Z}\exp\left[-\frac{\Delta G_U(T,x_U)-Fx_U}{k_BT}\right] \quad (5)$$

$$P_I = \frac{1}{Z}\exp\left[-\frac{\Delta G_I(T,x_I)-Fx_I}{k_BT}\right] \quad (6)$$

$$P_N = \frac{1}{Z}\exp\left[-\frac{\Delta G_N(T,x_N)-Fx_N}{k_BT}\right] \quad (7)$$

If we choose the reference state as I, then the partition function in Eq. (1) can be written as:

$$Z = \exp\left(-\frac{\Delta G_U(T,x_U)-Fx_U}{k_BT}\right) + \exp\left(\frac{Fx_I}{k_BT}\right) + \exp\left(-\frac{\Delta G_N(T,x_N)-Fx_N}{k_BT}\right) \quad (8)$$

From which we can rewrite the equilibrium probabilities as:

$$P_U = \left[1 + \exp\left(\frac{\Delta G_{UI}-F\Delta x_{UI}}{k_BT}\right) + \exp\left(\frac{\Delta G_{UN}-F\Delta x_{UN}}{k_BT}\right)\right]^{-1} \quad (9)$$

$$P_I = \left[1 + \exp\left(-\frac{\Delta G_{UI}-F\Delta x_{UI}}{k_BT}\right) + \exp\left(\frac{\Delta G_{IN}-F\Delta x_{IN}}{k_BT}\right)\right]^{-1} \quad (10)$$

$$P_N = \left[1 + \exp\left(-\frac{\Delta G_{IN}-F\Delta x_{IN}}{k_BT}\right) + \exp\left(-\frac{\Delta G_{UN}-F\Delta x_{UN}}{k_BT}\right)\right]^{-1} \quad (11)$$

where we have defined the convenient shorthand notations:

$$\Delta G_{UI} = G_U - G_I = -\Delta G_{IU}\ ;\ \ \Delta x_{UI} = x_U - x_I = -\Delta x_{IU}$$

$$\Delta G_{NI} = G_N - G_I = -\Delta G_{IN}\ ;\ \Delta x_{NI} = x_N - x_I = -\Delta x_{IN}$$

$$\Delta G_{UN} = G_U - G_N = -\Delta G_{NU}; \Delta x_{UN} = x_U - x_N = -\Delta x_{NU}$$

The fit to the occupation probabilities in Fig. 2C was obtained by fixing $\Delta x_{UN}$ = 31 nm from the extension distributions in Fig. 1D while treating all the other quantities as adjustable parameters.

The best fit was achieved with the values $\Delta x_{UI}$ = 15 ± 2 nm, $\Delta x_{NI}$ = 16 ± 1 nm, $\Delta G_{UI}$ = 16 ± 3 kcal/mol, $\Delta G_{NI}$ = 17 ± 1 kcal/mol, and $\Delta G_{UN}$ = 32 ± 3 kcal/mol.

**Zero-force free energy for NCS-1 conformers**

The comparison between the free energy differences calculated in single molecule experiments and in bulk experiments requires an estimate of the free energy needed for stretching the protein. If we indicate by $F_{1/2}$ the force at which states *U* and *N* have the same free energy, the zero-force free energy difference is (9, 10)

$$\Delta G^0_{UN} = F_{\frac{1}{2}} \Delta x_{UN} - \Delta G_{ST} = F_{\frac{1}{2}} \Delta x_{UN} - \int_0^{X_U} F(x')dx' \quad (12)$$

The elastic response of the protein is customarily represented by the worm like chain (WLC) model (11, 12) in which the relation between the force *F* applied to a molecule and its elongation *x* is given by

$$\frac{FP}{k_B T} = \frac{1}{4\left(1-\frac{x}{L}\right)^2} + \frac{x}{L} - \frac{1}{4} \quad (13)$$

Where *P* = 0.65 nm is the persistence length and *L* is the contour length, nominally computed as 0.36 nm per residue. Observe that $x_U = x_N + \Delta x_{UN}$, so for finding the zero-force free energy we need to know the length of the native state ($x_N$) of the protein. As such information is not available, we have used corresponding values from the $Ca^{2+}$ bound state of NCS-1, whose structure is known (13), confiding in the fact that the resulting systematic error is likely to be small in comparison with other sources of uncertainty. An alternative approach is to directly estimate $x_U$ by solving Eq. (13) at the force $F_{1/2}$: these two ways of estimating $x_U$ agree reasonably well, as we show in the following results. In the case of the $Mg^{2+}$-bound state of NCS-1 the handles are attached to residues 4 and 188, so we have *L* = 66.2 nm while $x_N$ = 3.5

nm from X-ray reconstruction of the $Ca^{2+}$-bound state. From Fig. 2C we get $F_{1/2}$ = 7.3 pN and from Fig. 1D we find $\Delta x_{UN}$ = 31 nm. With these numbers, Eq. (12) gives $\Delta G^0_{UN}$ = 16 ± 3 kcal/mol, to be compared with the bulk value of 11 ± 2 kcal/mol. For the apo state only the C-domain (residues 95-188) is folded in the native state, so we set $L$ = 33.5 nm and $x_N$ = 1.32 nm. Using the values $F_{1/2}$ = 6.5 pN and $\Delta x_{UN}$ = 14 nm from Figs. 3E and 3C, respectively, Eq. (12) yields $\Delta G^0_{UN}$ = 7.0 ± 1 kcal/mol, in good agreement with the bulk result 6 ± 1 kcal/mol. The alternative estimate of $x_U$ from inversion of Eq. (13) at force $F_{1/2}$ yields $x_U$ = 32.3 nm for the $Mg^{2+}$-bound state (compare with $x_N + \Delta x_{UN}$ = 34.5 nm) and $x_U$ = 15.1 nm for the apo state (while $x_N + \Delta x_{UN}$ = 15.3 nm).

**Equilibrium unfolding experiments**

We monitored the denaturation of NCS-1 by incubating in guanidine hydrochloride (GuHCl) followed by measuring intrinsic tryptophan fluorescence emission spectroscopy using a Perkin-Elmer LS50B spectro fluorimeter. Samples of 1-5 µM protein were prepared in 10 mM Tris, 250 mM NaCl, 10mM $MgCl_2$, 1 mM dithiothreitol, pH 7.0 with GuHCl concentrations in the range 0 - 8 M. The exact denaturant concentration of each sample was determined with a digital refractometer. All experiments were performed at ambient temperatures with excitation at 295 nm monitoring emission at 325 nm. The fraction of folded protein was calculated from the maximum and minimum intensities, and plotted against the concentration of denaturant. The data were fitted to three-state transitions as described (14).

$$f(x) = \frac{(a0+a1x)+(a2+a3x)*\exp(m1*\frac{(x-Cm1)}{RT})}{1+\exp\left(m1*\frac{x-Cm1}{RT}\right)} +$$

$$\frac{(a2+a3x)+(a4+a5x)*\exp(m2*\frac{(x-Cm2)}{RT})}{1+\exp(m2*\frac{(x-Cm2)}{RT}} \quad (14)$$

where a0, a1, a2, a3, a4 and a5 are the linear influence of denaturant on the different states, N, $[D_N N_C]$, D, respectively. At least 60 data points were used in each experiment.

**Supplemental Figures**

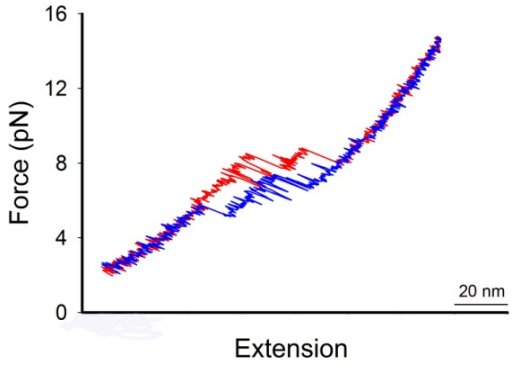


Figure S1. Mechanical manipulation of NCS-1$^{4\text{-}188}$. The protein was stretched (red trace) and relaxed (blue trace) at a constant speed of 20 nm/sec.

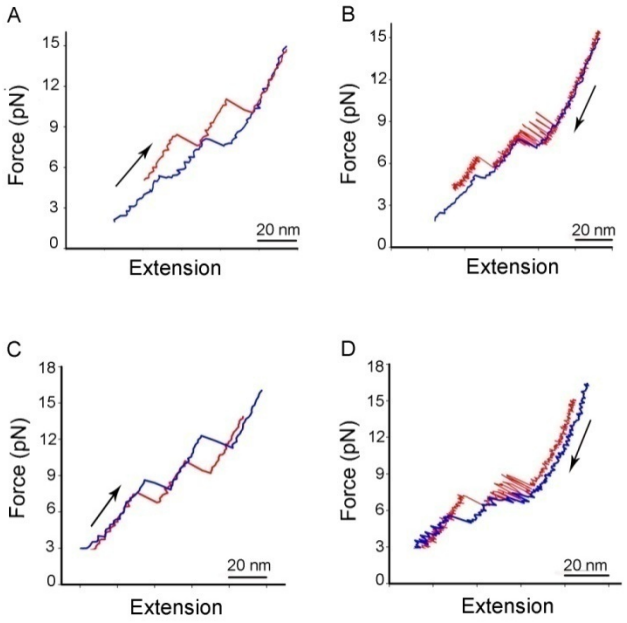


Figure S2. Asignment of unfolding/refolding transitions to individual domains. Stretching and relaxation traces for NCS-1$^{4\text{-}188}$ and two mutants designed to alter the size of the N- and C-domain individually. A) Superimposed stretching traces (100 nm/sec) acquired by pulling on NCS-1$^{4\text{-}188}$ (red) and NCS-1 $^{38\text{-}188}$ (blue). B) Superimposed relaxation traces (20 nm/sec) acquired by manipulating NCS-1$^{4\text{-}188}$ (red) and NCS-1 $^{38\text{-}188}$. Both in A) and B) the low force transition is smaller for NCS-1 $^{38\text{-}188}$. C) Superimposed stretching traces (100 nm/sec) acquired by pulling on NCS-1$^{4\text{-}188}$ (red) and NCS-1$^{10\ \text{Gly}}$ (blue). D) Superimposed relaxation traces acquired by manipulating NCS-1$^{4\text{-}188}$ (red) and NCS-1$^{10\ \text{Gly}}$. Both in C) and D) the high force transition is larger for NCS-1$^{10\ \text{Gly}}$.

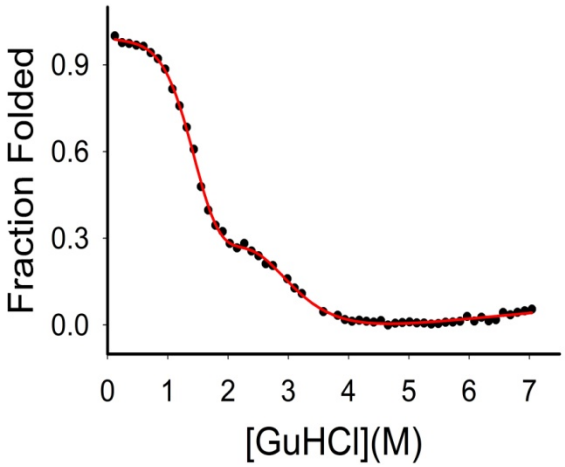


Figure S3.Equilibrium unfolding profile of wild type NCS-1 in 10mM $MgCl_2$.The solid line represents the best fit of the data to Eq. 14. The fitting of the data gave a global free energy change of unfolding of 11.0 ± 2.0 kcal/mol.

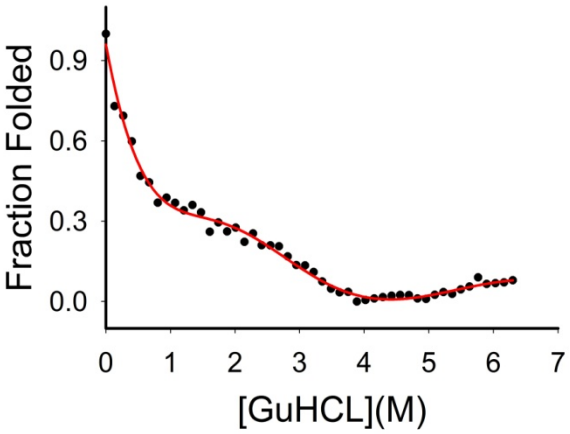


Figure S4.Equilibrium unfolding profile of wild type NCS-1 in absence of divalent ions. The solid line represents the best fit of the data to Eq. 14. The fitting of the data gave a global unfolding free energy change of 6.0 ± 1.0 kcal /mol.

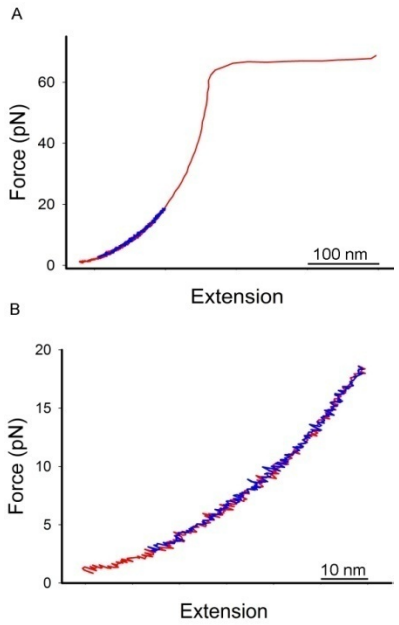


Figure S5. Mechanical manipulation of NCS-1$^{4-95}$. A) The protein was first stretched and relaxed three times at low forces (between 1 and 18 pN), and then the force was raised to induced the overstretching transition of the DNA handles at 67 pN, providing strong evidence for only one molecule being manipulated in the experiment. One stretching-relaxation cycle of panel A) is shown in panel B). The molecule was first stretched between 1 and 18 pN (red trace), and then relaxed to low forces (blue trace). The relaxation process was stopped at 2.5pN, before starting the next stretching-relaxation cycle, to avoid catching another tether at low forces. A total of 8 molecules were manipulated and 87 force vs extension cycles analyzed.

## SUPPORTING REFERENCES

1. Petrie LEBaT (1966) Statistical inference for probabilistic functions of finite state Markov chains. *The Annals of Mathematical Statistics* (37):1554-1563.
2. Rabiner L (1989) A tutorial on hidden Markov models and selected applications in speech recognition. *Proceedings of the IEEE*.

3. McKinney SA, Joo C, & Ha T (2006) Analysis of single-molecule FRET trajectories using hidden Markov modeling. *Biophysical Journal* 91(5):1941-1951.
4. Gao Y, Sirinakis G, & Zhang Y (2011) Highly anisotropic stability and folding kinetics of a single coiled coil protein under mechanical tension. *Journal of the American Chemical Society* 133(32):12749-12757.
5. Bell GI (1978) Models for the specific adhesion of cells to cells. *Science* 200(4342):618-627.
6. Tinoco I (2004) Force as a useful variable in reactions: Unfolding RNA. *Annu Rev Bioph Biom* 33:363-385.
7. Mossa A, Manosas M, Forns N, Huguet JM, & Ritort F (2009) Dynamic force spectroscopy of DNA hairpins: I. Force kinetics and free energy landscapes. *Journal of Statistical Mechanics: Theory and Experiment* 2009.
8. Gebhardt JC, Bornschlogl T, & Rief M (2010) Full distance-resolved folding energy landscape of one single protein molecule. *P Natl Acad Sci USA* 107(5):2013-2018.
9. Tinoco I & Bustamante C (2002) The effect of force on thermodynamics and kinetics of single molecule reactions. *Biophysical chemistry* 101-102:513-533.
10. Cecconi C, Shank EA, Bustamante C, & Marqusee S (2005) Direct observation of the three-state folding of a single protein molecule. *Science* 309(5743):2057-2060.
11. Bustamante C, Bryant Z, & Smith SB (2003) Ten years of tension: single-molecule DNA mechanics. *Nature* 421(6921):423-427.
12. Bustamante C, Marko JF, Siggia ED, & Smith S (1994) Entropic elasticity of lambda-phage DNA. *Science* 265(5178):1599-1600.
13. Heidarsson PO, *et al.* (2012) The C-Terminal Tail of Human Neuronal Calcium Sensor 1 Regulates the Conformational Stability of the Ca2+-Activated State. *Journal of Molecular Biology* 417(1-2):51-64.
14. Maxwell SL, Ho HY, Kuehner E, Zhao S, & Li M (2005) Pitx3 regulates tyrosine hydroxylase expression in the substantia nigra and identifies a subgroup of mesencephalic dopaminergic progenitor neurons during mouse development. *Developmental biology* 282(2):467-479.